Thermal Contact Conductivity Prediction with Grey Box Model and Experimental Validation for an Axial Flux Motor

Zhaozong Li
National Engineering Laboratory for
Electric Vehicles and School of
Mechanical Engineering
Beijing Institute of Technology.
Beijing, China
zz_li312018@163.com

Chengning Zhang
National Engineering Laboratory for
Electric Vehicles and School of
Mechanical Engineering
Beijing Institute of Technology.
Beijing, China
mrzhchn@bit.edu.cn

Fengyu Zhang
Power Electronics, Machines and
Control Research Group and Faculty of
Engineering
University of Nottingham
Nottingham, United Kingdom
ezzfz2@exmail.nottingham.ac.uk

Zeyuan Xu
Power Electronics, Machines and
Control Research Group and Faculty of
Engineering
University of Nottingham
Nottingham, United Kingdom
epzzx@exmail.nottingham.ac.uk

David Gerada
Power Electronics, Machines and
Control Research Group and Faculty of
Engineering
University of Nottingham
Nottingham, United Kingdom
ezzdg2@exmail.nottingham.ac.uk

Chris Gerada
l Power Electronics, Machines and
Control Research Group and Faculty of
Engineering
University of Nottingham
Nottingham, United Kingdom
eezcg@exmail.nottingham.ac.uk

Xueping Li
National Engineering Laboratory for
Electric Vehicles and School of
Mechanical Engineering
Beijing Institute of Technology.
Beijing, China
lixueping6677@163.com

Shuo Zhang
National Engineering Laboratory for
Electric Vehicles and School of
Mechanical Engineering
Beijing Institute of Technology.
Beijing, China
shuozhangxd@163.com

Yue Zhao
National Engineering Laboratory for
Electric Vehicles and School of
Mechanical Engineering
Beijing Institute of Technology.
Beijing, China
zhao_y2020@106.com

Abstract—**Axial Flux Permanent Magnet Synchronous Motor (AFPMSM) attracts increased attention in recent years due to the inherent high torque density. The yokeless and segment armature is one of the most advanced structures, with reduced axial length and increased efficiency. For the segment armature fixed axial flux motors, encapsulating material is required between the winding and the structure fins. However, it is difficult to calculate the contact thermal conductivity between the fins and windings for the machine thermal performance prediction, due to the multiple material components and different interface pressure. For the complicated materials characteristics analysis, Grey Box theory is proposed to predict the thermal behavior of the non-metallic mixture in the contact region in this paper. Firstly, the axial flux motor topology is presented, as well as a single sector model. Then the Grey Box frame is introduced with the testing rig to train the critical parameters that will be used in thermal model. Through genetic algorism, the thermal conductivity and heat capacity of mixture materials in the area of the segmented armature contact surface are obtained. Finally, the equivalent thermal conductivity in the contact region is updated to a 3D thermal model, which are experimentally validated on a sector model and a prototype motor.**

Keywords—Axial Flux Motor, Segment Armature, Encapsulating Material, Grey Box Theory

I. INTRODUCTION

In the direct drive systems, due to the compact axial structure and high torque density, Axial Flux Permanent Magnet Synchronous Motor (AFPMSM) has attracted widespread attention. One key challenge is the heavy thermal load at the armatures and the encapsulation, which will affect the reliability of the machine, insulation level, and result in damaged potting material or PM demagnetization. Cooling systems have been introduced in literatures [1-3] to help dissipate the heat generated in the coil. However, the thermal contact resistances between the armatures and fins remain to be determined to predict the coil temperature. Most of the thermal models in previous existing literatures ignore the thermal resistance at this interface or only apply a lower value of thermal conductance to ensure the reliability of the motor [2-3]. In addition, although the total heat dissipation in a single sector is easy to test by an experiment, the thermal distribution is different in each position due to the material composition, the pressure and epoxy flow conditions. So the difference in heat transfer performance at different locations is difficult to be determined. Therefore, further research on the equivalent conductance at this area is required.

At present, some scholars are using the FEM and multi-field coupling to conduct the thermal analysis on electrical machines [2-6], which are mostly based on the empirical parameters with limited consideration for the encapsulating materials and the tolerance of armature assembly. For the Lumped Parameter Thermal Network (LPTN) method [7-9] and the transient temperature prediction [7], the empirical parameters used for the encapsulating materials are limited as well, it is difficult for researchers to obtain accurate information on the contact surface. Furthermore, during the sector insertion process, static pressure, ambient temperature, epoxy viscosity and the properties of the slot liner will all have impact on the contact thermal resistance and thus the thermal model. Recently researchers have come up with the Grey Box (GB) theory and low-order model which can be applied to solve the thermal interface problem with multi-unknown parameters in consideration and build up an equivalent resistance in a variety of uncertain materials [10-11]. In [11], the genetic algorithm (GA) is mentioned to fine-tune the uncertain thermal resistance, which has been well verified in

a multisector three-phase machine. In previous literature [12], it mentioned the method of evaluating winding impregnation using a DC source experiment. The complex influence of the processing technology on the thermal behavior of the winding is analyzed, and the powdered thermal insulation material is used in the experiment to control the heat dissipation path of the winding. Finally, the result is embedded in the thermal resistance network, and a significant result is obtained. Compared with the Black Box, the most significant advantage of the Grey Box is that it can implant the known information and reasonable conjectures into the framework in advance. Therefore, the boundary conditions can be furtherly set for more more accurate result.

Therefore, it can be concluded as, the GB theory can not only increase the calculation speed, simplify the complex problems, but also make it easier to use the algorithm in models to fine-tune the thermal conductivity on nonideal conditions. In this paper, the authors establish the heat transfer path of the motor, and determine the non-metallic materials and related parameters that need to be included in the GB. Based on the experiments of a single sector sample with DC power, data has been collected as machine learning sources for training the GB and fine-tune the coefficient in the frame to get the equivalent resistance. Compared with the previous literatures, the innovation of this article is mainly reflected in:

1. A GB model is constructed at the contact surface of the segmented armature and heat dissipation fins of the axial flux motor, which provides an abstract space for the mixed medium of various materials.

2. GA is introduced to perform a global fine-tune method. The thermal properties of various materials provides a certain scope for the search domain while the fine-tune program to avoid the over-coupling.

3. The thermal behavior of the contact surface under transient conditions is obtained by tuning the thermal conductivity and heat capacity within the acceptable range.

Finally, the obtained result of contact thermal conductivity is applied to a single sector model to prove the available of this method. The model of single sector model is finally embed in a traditional 3D-LPTN model build for the studied axial flux machine to predict the machine thermal performances. All results will verified by the experiment.

II. STUDIED OBJECT

A. Studied Motor

Generally, the AFPMSM have single-rotor double-stator and single-rotor single-stator structures. The above stator design method also appears in many literatures [1][4][7], and it is a design idea with high torque density in the current axial flux motor. Figure 1 shows the exploded view of the studied dual-rotor and yokeless and segment armature stator motor. The motor cores are made of oriented silicon steel sheets, with cylindrical copper wires wounded coil. The heat dissipation fins are made of aluminum alloy [HE30TF] with double liquid tubes. The segmented armatures are inserted and fixed with epoxy resin, which is the Epoxy lite 235SG with high mechanical strength and high temperature resistance. Meanwhile, with the yokeless and segment armature topology, fractional slot and concentrated winding are used in the motor.
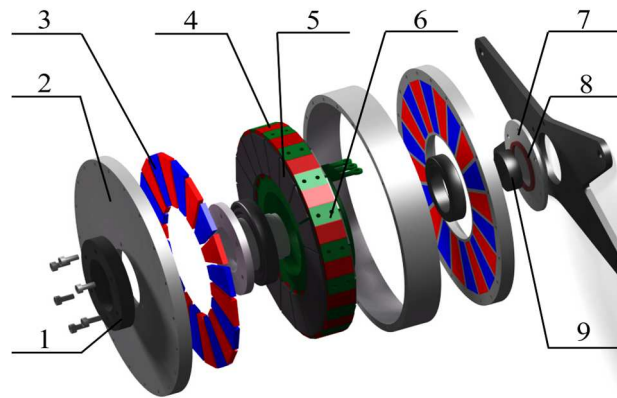

Figure 1. Topological Structure

1-Flange, 2- Rotor Housing, 3-PMs, 4-Segment Armature, 5-Cores, 6-Liquid Cooling Fins, 7-End Cup, 8- Bearing Fastening Ring, 9-Rotary Transformer

The critical parameters related to the thermal field and 3D-LPTN model of the motor are listed in Table 1.

Table I - Critical Parameters of the AFPMSM

Parameter	Value	Unit
Rated Power	150	kw
Bus Voltage	800	V
Rated Torque	475	Nm
Synchronous Speed	2600	r/min
Winding Outer Radius	176	mm
Winding Inner Radius	93	mm
Slot Number	18	/
Pole Number	20	/

B. Thermal Conductivity on Conact Surface

Even though this kind of yokeless segmented armature axial flux motor with dual rotors has a high torque density, the accompanying problem is that the heat dissipation path of the stator is single, usually only through the cooling fins [1] [2] as well as the cooling liquid within to for the armature temperature minimization. Therefore, the heat transfer conditions of this contact surface have become a hot spot in the study of the temperature field of this kind of motor, and the thermal conductivity of this area has become difficult due to the complex conditions of the contact surface.

Figure 2 shows the cross-section of the segmented armature winding and fins, and the white dashed box is the contact position studied in this paper. In order to simplify the thermal resistance model of this surface, the structure of the cooling pipes is omitted in Figure 2.
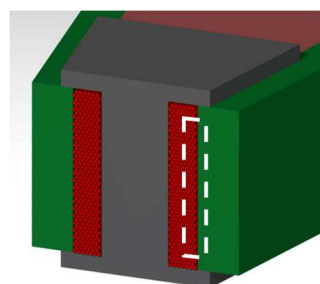

Figure 2. Cross-Section of a Single Sector

This area is the critical thermal resistance that determines the heat dissipation efficiency of the segmented armature and

the main research object is this paper as well. It can be concluded as that one side of this area is the main heat generating part of the motor stator and the other is the main cooling location, which directly connects the heat generation of the stator and the coolant in the cooling fins. And on both sides of this area, the previous research have given an acceptable solution of the thermal behavior [13][14]. The materials at the interface include enamel wires, epoxy, slot liner and air bubbles. Due to the manufacturing process and unbalanced pressure between the winding and the fin. The empirical parameter to predict the contact resistance is not adequate for the accuracy requirement, which requires further research.

Based on the manufacturing method of stator in segmented armature AFPMSM, the contact thermal conductivity has become the most difficult part in building the motor thermal model, which can be summarized into two aspects as follow. Indeterminate heat transfer thickness and indeterminate material composition. The reason comes from the difficulty to determine the microscopic thickness of various materials at this position, and the contact surface is not an ideal plane either. In addition, different types of windings will also lead to different flatness on the coil surface. So the equivalent medium theory is hard to apply in this area and the LPTN method cannot establish a grid of heat transfer characteristics in a small and complex space either [7]. On the other hand, the difference in craftsmanship will also have a serious impact on the thermal resistance of the contact surface during the insertion of the segmented armature, and it is difficult to evaluate the pros and cons of the craftsmanship through mathematical methods.

In this paper, the main components of the white box area are enamel wire, epoxy resin, and insulating liner. In previous literatures, the equivalent thermal conductivity of the contact surface between the windings and cooling fins usually refers to the epoxy resin (0.2~0.9W/m·k) [2-5]. However, it is still a wide range to use in a model and the value can be affected by the aforementioned manufacturing process, as well as the material properties that maybe different from the datasheet. Therefore, it is necessary to propose a model to calculate the reasonable thermal conductivity of this area.

III.   GREY BOX MODEL

A. Thermal Behavior on the Contact Surface

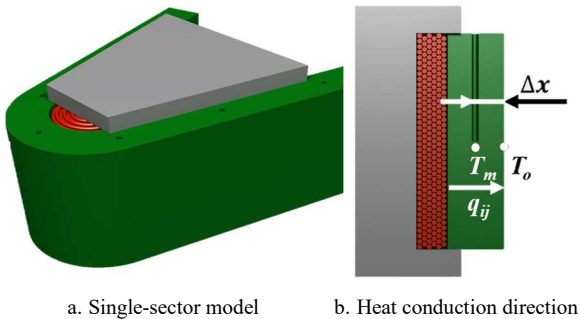a. Single-sector model   b. Heat conduction direction

Figure 3. Single sector model

The single-sector temperature model after omitting the cooling liquid pipe is shown in Figure 3a, including the stator core, winding coil, heat dissipation fin, and non-metallic materials on the contact surface. The direction of heat flow q_{ij} of the winding is shown in Fig. 3b. Where, T_m is the temperature of the middle point of the cooling fin, T_o is the temperature outside the model, Δx is the distance between T_m and T_o, ij represent different working condition. According to the Fourier heat transfer equation (1), q_{ij} can be calculated by T_m and T_o.

$$q_{ij} = \lambda_{Al} A \frac{T_m - T_o}{\Delta x} \qquad (1)$$

where, A is the surface area of the heat dissipation fin, λ_{Al} is the thermal conductivity of aluminum alloy [HE30TF]. In order to reduce the uncertain factors in the model and ensure the accuracy of the subsequent construction of the GB model, it is necessary to control q_{ij} as the only heat transfer path of the sample.

Based on the analysis of the single sector heat dissipation, the author modified the thermal isolation material for the sample as shown in Figure 4 in order to control the heat transfer path. Therefore, the multidirectional heat dissipation behavior can be limited within a specific U shape contact surface. And the grey box will be established in this contact area.
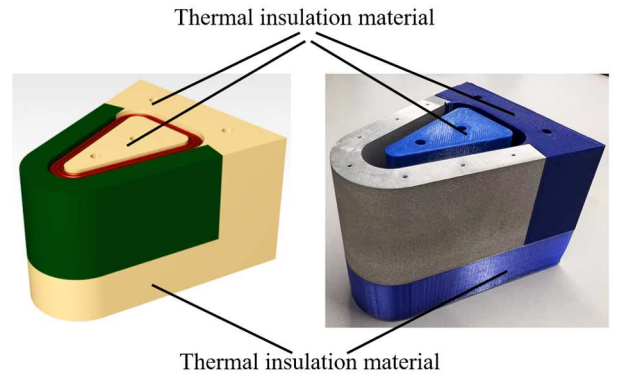
Figure 4. Arrangement method of thermal insulation material
*In order to make it easier to see where the windings are located, the symmetrical isolating tooth yoke at the top is temporarily removed.

At the same time, for the convenience of the experiment, the volume of the model is 1/2 of the actual armature, and the static pressure of the coil inserted into the cooling fin is also 1/2 of the stator assembly. The materials used in the samples are the same as the studied motor. The known thermal resistance in the single-sector model is shown in Table 2, which can be directly used in the thermal model.

Table II – Thermal Conductivity of the Materials

Item	Value
Bare Copper	401 W / m·K
Aluminum [HE30TF]	180 W / m·K
Enamel	0.81 W / m·K
Isolation Liner	0.34 W / m·K
Epoxy lite 235SG	0.26 W / m·K

With the arrangement of the insulating material, the heat flow between T_m and T_o can be used to estimate the thermal conductance around the heat dissipation fin. In order to collect a more accurate temperature distribution, 7 collection points are set on both sides of the U-shaped cooling fin, the average of the two symmetrical points will be taken at one data, except for the end zone. It should be noted that the thermal insulation material can only guarantee the heat transfer direction in the 2D model, but the single-sector 3D thermal model also has heat transfer along the winding cooling, along the U-shaped

fin and other directions, so it is still necessary to build a complete 3D- LPTN model in the single-sector model as shown in Figure 5, which can achieve accurate heat flow calculation in one direction.
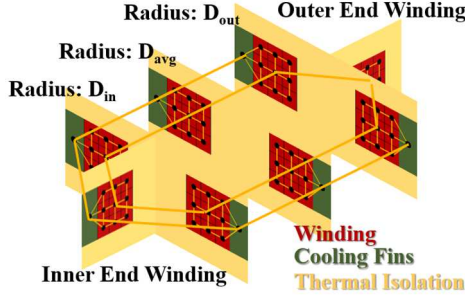

Figure 5. 3D-LPTN of a Thermal Isolate Sector

The three radial positions and the end windings selected in the model are designed to represent the difference in the contact thermal resistance at different positions, in order to fit the collect the temperature of seven positions on the cooling fin. Through the previous literatures, the thermal resistance of the winding in all directions has been fully studied [7][13], and the heat dissipation fin is a metal with known properties, but the critical problem is the thickness of contact area is not known for the designers. The reason is the thickness of the contact surfaces cannot be determined mathematically or by evaluating the machining process, these planes are not even two parallel surface, as shown in Figure 5.
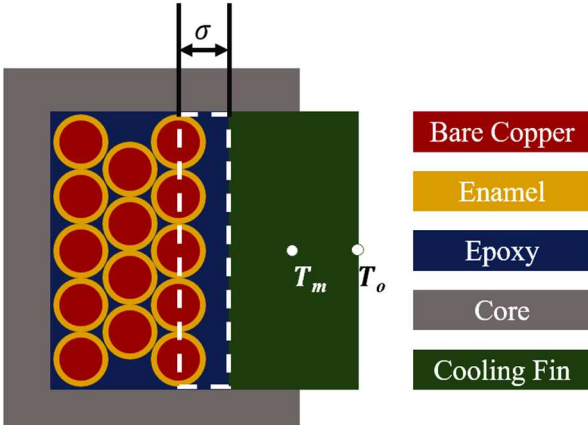

Figure 6. Actual Situation of Segmented Armature Contact Surface

Therefore, it is difficult to directly calculate the thermal conductivity in this area. And the main significance of the grey box here is that it can express the thermal resistance for which the distance cannot be determined, and build a weighted graph model within a sector that does not involve the thickness of the winding.

B. *LPTN in a Single Sector*

In the micrograph at the cogging surface shown in Figure 6, the steady-state framework for 3D-LPTN in Figure 5 can obtain as (2):

$$P_i = \sum_{j \neq i} (T_i - T_j) g_{ij} \tag{2}$$

The matrix form is in (3):

$$\begin{bmatrix} P_1 \\ \vdots \\ P_N \end{bmatrix} = \begin{bmatrix} \sum_{j \neq 1} g_{1j} & \cdots & -g_{1N} \\ \vdots & \ddots & \vdots \\ -g_{N1} & \cdots & \sum_{j \neq N} g_{N1} \end{bmatrix} \begin{bmatrix} \Delta T_1 \\ \vdots \\ \Delta T_N \end{bmatrix} \tag{3}$$

Where P_i is the heat generated in ith node, T_i and T_j are the temperatures of the ith and jth nodes respectively, and g_{ij} is the thermal conductance between the ith and jth nodes. This model has been widely used by researchers. In order to furtherly improve the practicability of the model and the ability to predict the transient temperature, the calculation method including the heat capacity is introduced into 3D-LPTN as shown in (4)

$$P_i = \sum_{j \neq i} (T_i - T_j) g_{ij} + C_i \frac{dT_i}{dt} \tag{4}$$

The matrix form is in the (5):

$$\begin{bmatrix} P_1 \\ \vdots \\ P_N \end{bmatrix} = \begin{bmatrix} \sum_{j \neq 1} g_{1j} & \cdots & -g_{1N} \\ \vdots & \ddots & \vdots \\ -g_{N1} & \cdots & \sum_{j \neq N} g_{N1} \end{bmatrix} \begin{bmatrix} \Delta T_1 \\ \vdots \\ \Delta T_N \end{bmatrix} + \begin{bmatrix} C_1 \frac{dT_i}{dt} \\ \vdots \\ C_n \frac{dT_N}{dt} \end{bmatrix} \tag{5}$$

where, C_i is the thermal capacitance. It only affects transient temperature changes. They can be calculated from mass or volume and specific heat capacity, and can be dispensed exactly according to the respective material's data sheet. According to the first law of thermodynamics in (6):

$$\frac{\Delta E_{in}}{dt} = \frac{dQ_i}{dt} - \sum (g_{ij}(T_i - T_j) + \frac{C_i \cdot dT}{dt}) \tag{6}$$

where, ΔE_{in} is the change in the internal energy of the winding, and Q_i is the total heat input from the external power supply. Therefore the subsequent GB can be controlled by the DC power supply to control its temperature state.

C. *Grey Box Frame*

In a 3D-LPTN model, the format of the critical parameter is the node thermal conductivity that can be directly embedded in the whole model. Therefore, the optimal form of thermal conductivity at the contact surface between the coil and the cooling fin should also be a model that facilitates the efficient connection with the thermal resistance network of other parts of the AFM stator. As in the previous analysis of the LPTN model, the thermal network of the fins and the windings are clear, the size of the space in the slot is also known. Therefore, this paper specifies a representative space to express the contact thickness, so as to facilitate the calculation of the thermal resistance of the model and the portability of the thermal resistance this paper studied. Therefore, in order that this parameter can be embedded in any motor thermal model later, this paper defines the space for the trained thermal resistance, that is the thickness on the contact surface, but the material composition in this space is unknown. And the significance of the GB used here is they can simultaneously locate the accurate values of thermal conductivity and specific heat capacity in the contact area with uncertain parameters. In this paper, the authors build 7 GB models, as shown with the thick solid lines in Figure 7. $\{G_a, G_b, G_c, G_d, G_{c'}, G_{b'}, G_{a'}\}$ represent the thermal conductivity in their abstract distance of

each position respectively, and Symmetrical points will be averaged while the model is being applied.
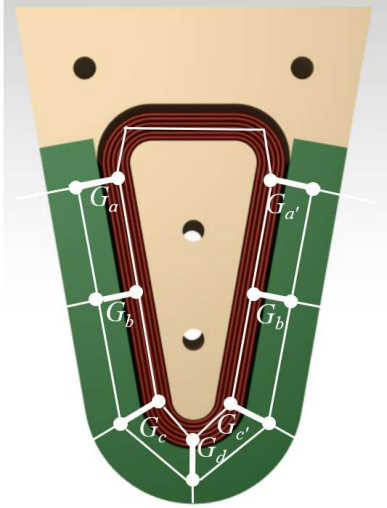

Figure 7. Weighted Graph in a Single Sector

On the basis of GB space, independent variables and dependent variables need to be set to provide more machine learning data. So as to ensure that the thermal conductivity searched in the specified space has practical value. This article refers to the variables in the actual working environment of the segmented armature, one is the losses generated within the winding, and the other is the inlet temperature and the flowrate of the coolant. So far, the state group power i and the external environment j are established, representing the state matrix of different losses in the coil and different coolant temperatures around the heat sink, respectively. The corresponding fine-tuning variable is the thermal conductivity in $\{G_a, G_b, G_c, G_d, G_{c'}, G_{b'}, G_{a'}, \}$. Based on the GB frame and independent variables, The dependent variable selects a parameter that the designer is most concerned about, the heat taken away by the cooling fin $\{q_i\}$ in this seven position.

In order to improve the calculation speed and the reliability of the results, the relationship between the independent dependent variables in the GB should be built as clear as possible. At the same time, the machine learning data of the vector is also more conducive to the solution of the intermediate position parameters. According to demand of LPTN building process, the GB sets the input matrix **X** of the space as the heat production of the winding, which is controlled by the DC power supply. The output matrix **Y** is the heat flux in 7 positions of the cooling fin. The frame of training process is shown in Figure 8.
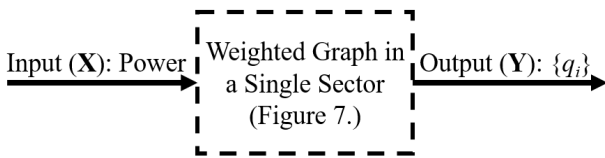

Figure 8: Grey Box on the Contact Surface

D. Fine-tuning with Genetic Algorithms

Figure 9 shows the method of obtaining the machine learning data. The angle of this sector refers to the actual situation of the 18-slot motor, the armature angle is 20°, and the static pressure of the insertion set as 40N perpendicular to

the axis of the motor. The temperature outside the sample is provided by the water tank of the incubator.
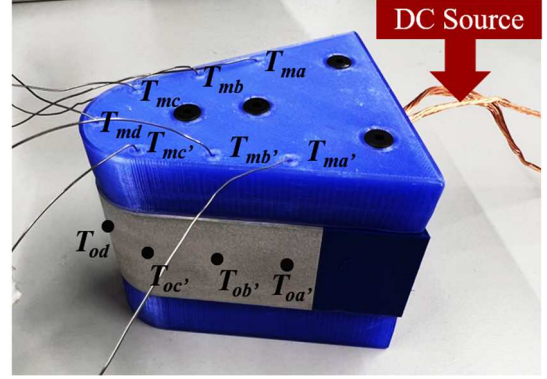

Figure 9. $\{q_i\}$ Measuring Rig

Figure 10. Pico with 14 Channels

With the device shown in Figure 10, it is possible to directly measure the temperature gradient in the cooling fin at various locations on the sample. The test process requires measuring the steady state temperature rise state under different constant power input conditions. In the face of matrix equations with lots set of G_{ij} and C_i, it is usually difficult to obtain the accurate solutions with the mathematical methods. So this paper introduces genetic algorithms to obtain their global suboptimal solutions. Therefore, it is necessary to obtain the relevant temperature information, which will be used as learning data for machine, and the information needs to be carried out under transient conditions as well. Each node in LPTN conductance (5) has actual physical meaning that proves the feasibility of the enumeration method. The operation process of the genetic algorithm is shown in Figure 11.
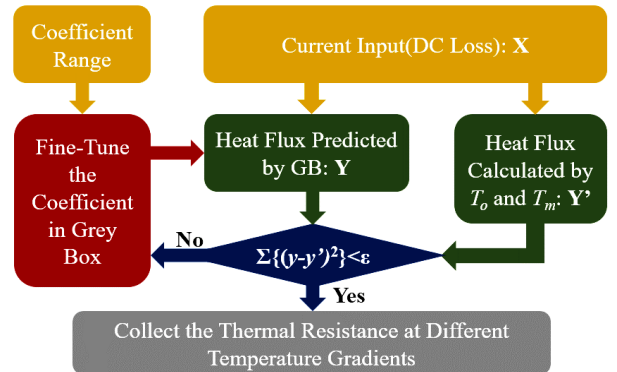

Figure 11. The GA Process

In Figure 11, **X** is the matrix of input current. **Y** and **Y'** are the heat flux in each position predicted by the GB model and the heat flux calculated by the (T_o, T_m) respectively. Under the corresponding state of the specific current excitation, x_i, y_i and y'_i in each matrix can be uniquely determined. The framework to get **Y** matrix by GB is shown in (7)

$$[Y] = f_\xi \{x_1, x_2 \cdots x_N\} \qquad (7)$$

where, f_ξ is the function form like Figure 7. **Y** is the heat flow at 7 positions obtained by the input current at different operating points through the function. Meanwhile, **Y'** will be measured in pairs with **X** during the experiment as $\{x_n, y_n\}$. These values will fine-tune the coefficient in f_ξ as a GA learning source, with the iteration formula in (5), and the expectation model is shown in (8):

$$\sum min\{(y - y')^2\} < \varepsilon \qquad (8)$$

Therefore, according to the properties of the materials in Table 2, the paper first presents the range of the training thermal conductivity results to avoid overfitting. In the predicted GB model, the maximum thermal conductivity of each position is the transverse empirical thermal conductivity of the winding, and the minimum value is the thermal conductivity of the insulating paper. Therefore, the range of g_{ij} is (0.2~12.5W/m·k). C_i is same in the empirical range, and the value range refers to the bare copper and isolation material (0.39~1.85J/g·k). However, the specific heat capacity in units of gram is not convenient to use in the model, so the units are converted to volume ratios (1.21~3.51J/cm³·k). The two parameters are divided into 10 partitions within this range, and 100 initial conditions are taken in each region, In the GA calculation, 1024 ant colony calculations were performed.

Based on the above algorithms, the content of machine learning will be provided by experimental data. During the experiment, the power of the DC power supply was changed 10 times, and the temperature of the cooling fin in contact with the cooling liquid was adjusted 5 times at the same time, so as to obtain 50 sets of learning data. In order to improve the portability of the GB model, 1mm of the contact surface is set as the "contact thermal resistance", and the rest are the coils and cooling fins. The thickness of the rest of the model only needs to be subtracted from the outer contour by the thickness of the junction. After the training process, the thermal conductivity and specific heat capacity of the hybrid material within 2 mm were obtained.

Table III –Results of the Fine-tuned process

Position	Conductivity (w/m·k)	Capacity(J/cm³·k)
a	0.26	1.4
b	0.84	1.3
c	3.42	2.2
d	0.25	1.4

It needs to be clear here that the above thermal conductivity and specific heat capacity are not the specific properties of a certain material, but the thermal behavior of the mixed medium in a set area. Meanwhile, it can be noticed that the thermal conductivity of point c is significantly higher than that of other positions. The reason for this phenomenon is that the 1mm thickness area at position c includes copper, but this does not affect the subsequent using of GB.

IV. EXPERIMENTAL VALIDATION

A. Single Sector Validation

To verify the reliability of the above values, the method was first applied to a single-sector sample. In this verification process, in order to be more in line with the actual working state, in the above single-sector model, the traditional silicon steel sheet is used to replace the iron core made of thermal insulation material, and a real single-sector model is established, as shown in Figure 12. The input quantity in the experiment is still a constant current power supply, and the sample is placed in a constant temperature environment to better apply the data obtained by the above GB model.
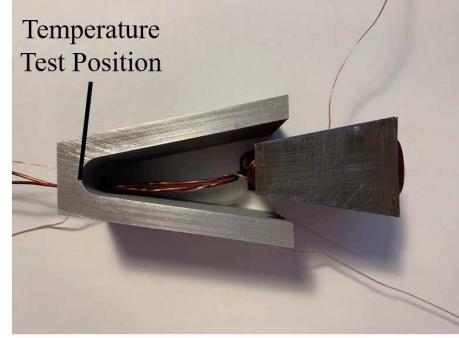

Figure 12. Single Sector Model

The 3D-LPTN model of the single sector model is shown in Figure 13. The idea of modeling follows the theory of the split-ring method in the axial flux motor [7][9]. The main principles of modeling are as follows. One is to express the complex thermal behavior in the motor stator with the most concise thermal resistance mesh and improving the portability of single-sector 3D-LPTN. The other is to better embed the thermal conductivity of the contact surface, so as to reflect the result of the genetic algorithm fine-tune process of the GB.
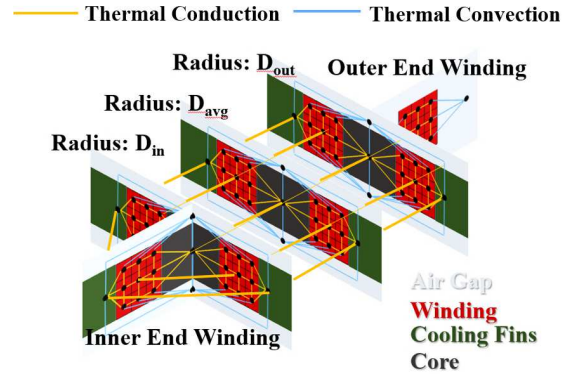

Figure13. 3D-LPTN of the Single Sector

Figure 13 is a 3D-LPTN model of the single sector model above. The model establishes three 2D-LPTNs at different specific radius and the end winding, which involves the thermal resistance and thermal capacitance of the four positions of a, b, c, and d. And it can be found from the model that the single-sector 3D-LPTN top view is the previously trained GB model as shown in Figure 7, and the sector model established by the split-ring method is also closer to the actual motor than the thermal model in Motor-CAD's geometry structure. After the above optimization, the most notable feature is the nodes of irrelevant positions are reduced in the model, like the node of the heat dissipation fin is also set to

one, because relative to the temperature of the winding, the temperature distribution in them is usually not the designer's concern. As a result, the interface between the heat dissipation fin and the winding is more clear and the GB parameters can be easily embedded in this model. The heat conduction relationship in the model can be divided into: heat transfer between the stator core and the winding, inside the winding, and between the winding and the cooling fin. The heat convection includes the heat dissipation of the silicon steel sheet, the heat dissipation fin and the outer end winding. Heat radiation was omitted from this experiment because of its small contribution to the case study being investigated.

According to the contact surface thermal resistance and specific heat capacity parameters given in Table III, the 3D-LPTN model of a single stator sector is re-established. The temperature of the node at the minimum radius was evaluated in the transient state and thermal steady conditions. According to the predicted curve and experimental data of the LPTN with GB model in Figure 14. The value is in a good agreement with the measured temperature, and the maximum error is 6.5%, which appears in the heating stage of 160s, the absolute value is 4.2°C, and the steady-state average error is about 3°C. This demonstrates the effectiveness of the GB and genetic algorithm in the fine-tuning process of LPTN in transient temperature prediction can be applied.
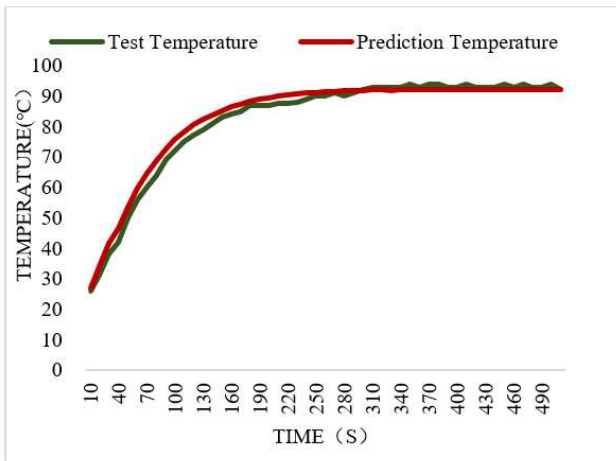

Figure14. Temperature in a Single Sector

B. Machine Model Verification

In order to further prove the validity of this parameter, the author verifies its validity in the 3D-LPTN of the whole machine. The test rig is shown in Figure 15.

Figure 15. Experiment Bench

*The location of the thermocouple arrangement is at the inner diameter of the coil like Figure 12, which is usually the best location for the temperature check of the axial flux motor.

The temperature test point of the whole machine experiment is the same as the single-sector temperature test, which is the smallest radius of the stator armature, because this position has the largest thermal load in the motor stator. The thermal resistance network of the stator is based on the single-sector model with addition liquid cooling pipe thermal conductance path[8] and air gap heat convection [11] in the motor. The model follows the construction method of the thermal resistance grid model of the motor in [7] and the GB parameters in the sector.

The final model of the whole machine uses the centrosymmetric properties of each sector in axial flux motor to obtain the three-dimensional thermal resistance network of the 18-slot stator of the whole machine. The experiment tested the temperature rise under 100kw and rated power of 150kw respectively. The laboratory room temperature is 22.5°C, the inlet temperature is 20°C, and the flow rate is 25L/min. The model prediction curve and measured temperature under 100kw and 150kw power are shown in Figure 16 and Figure 17, respectively.
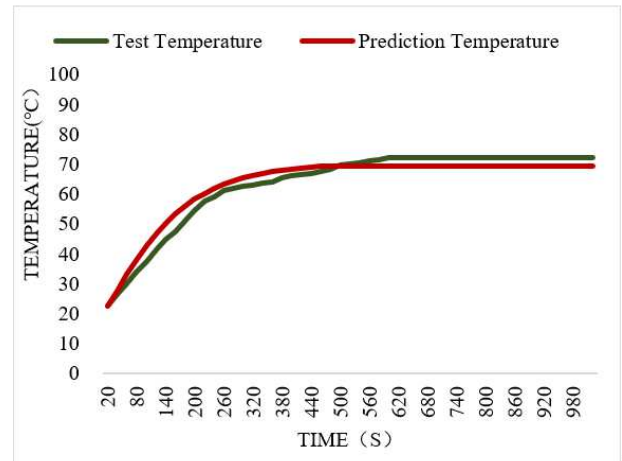

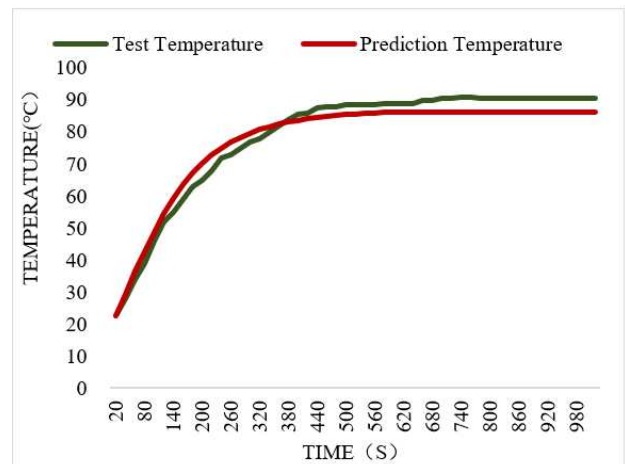Figure16. Temperatures in 100kw

Figure17. Temperatures in 150kw

The data in Figure 16 and Figure 17 show that the model predicted temperatures at different powers are in good agreement with the experimental results. The 3D-LPTN embedded in the GB model broadens the working state of the traditional LPTN model and realizes the temperature prediction in the process of motor temperature rise. Finally, after introducing the algorithm fine-tune, the maximum

transient error of the LPTN with GB is 8.8°C, and the steady-state errors under the two powers are 3.6°C and 6.7°C, respectively. After the analysis of the samples, the source of the error may exist in the search error of the d-point GB model. Because the end of the coil cannot fully contact the cooling fins, the set thickness of 1mm contact surface may not cover the entire non-metallic part.

Since the reliability of the motor has not been verified, it is not possible to conduct experiments in the overloaded working area. However, through the results of the two operating points, a good agreement between the predicted value of LPTN and the measured temperature can already be expressed, which proves the feasibility of replacing part of the complex nodes with GB in the thermal resistance network. It also proves that it makes sense to search GB using a genetic algorithm. In the end, the establishment of the GB model and the genetic algorithm made it clear that the thermal resistance of the critical position, and which is difficult to obtain in the experience parameters, can be got with constructing a scaled-down sample with the same material. The thermal behavior of the parts with unclear material properties can be expressed by GB, and this uncertain model can be searched using genetic algorithms as well.

V. CONCLUSION

This paper demonstrates the feasibility of using the GB model to predict the contact resistance between fins and windings, which is difficult to determine in traditional thermal method. At the same time, a method to fine-tune GB by means of scaled-down samples and genetic algorithm is proposed. Finally, the equivalent thermal conductance values and heat capacities obtained in the GB were applied to the 3D-LPTN thermal model to predict the armature temperature of the machine. From a direct comparison of the experimental data, it can be seen that the GB method provides a good estimate of the thermal conductivity of the interface between the coil and the fin and is also well suited for embedding into some LPTN models. In future research, the authors will continue to explore how the method can extract critical information in a single-sector model in the face of different sector angles (slot numbers) and different stresses, hoping to use static pressure and sector angle as the independent input variables of the GB model to build the stator model. And research on whether the mathematical relationship between thermal resistance and insertion stress, enabling faster prediction of overall machine temperature for a wider application GB model to axial flux motors.

REFERENCES

[1] H. Vansompel, P. Leijnen and P. Sergeant, "Multiphysics Analysis of a Stator Construction Method in Yokeless and Segmented Armature Axial Flux PM Machines," in IEEE Transactions on Energy Conversion, vol. 34, no. 1, pp. 139-146, March 2019, doi: 10.1109/TEC. 2018.2862622.

[2] S. Nategh, A. Krings, O. Wallmark, and M. Leksell, "Evaluation of impregnation materials for thermal management of liquid-cooled electric machines," IEEE Trans. Ind. Electron., vol. 61, no. 11, pp. 5956–5965, Nov. 2014.

[3] P. Lindh et al., "Direct Liquid Cooling Method Verified with an Axial-Flux Permanent-Magnet Traction Machine Prototype," in IEEE Transactions on Industrial Electronics, vol. 64, no. 8, pp. 6086-6095, Aug. 2017.

[4] R. Wrobel, G. Vainel, C. Copeland, T. Duda, D. Staton and P. H. Mellor, "Investigation of Mechanical Loss Components and Heat Transfer in an Axial-Flux PM Machine," in IEEE Transactions on Industry Applications, vol. 51, no. 4, pp. 3000-3011, July-Aug. 2015, doi: 10.1109/TIA.2015.2405499.

[5] F. Marignetti, et al., "Design of Axial Flux PM Synchronous Machines Through 3-D Coupled Electromagnetic Thermal and Fluid-Dynamical Finite-Element Analysis," in IEEE Transactions on Industrial Electronics, vol. 55, no. 10, pp. 3591-3601, Oct. 2008.

[6] B. Zhang, T. Seidler, R. Dierken and M. Doppelbauer, "Development of a Yokeless and Segmented Armature Axial Flux Machine," in IEEE Transactions on Industrial Electronics, vol. 63, no. 4, pp. 2062-2071, April 2016, doi: 10.1109/TIE.2015.2500194.

[7] R. Burke, A. Giedymin, Z. Wu, H. Chuan, N. Bourne and J. G. Hawley, "A Lumped Parameter Thermal Model for Single-Sided AFPM Machines With Experimental Validation," in IEEE Transactions on Transportation Electrification, vol. 6, no. 3, pp. 1065-1083, Sept. 2020, doi: 10.1109/TTE.2020.2998110.

[8] F. Zhang et al., "Electrical Machine Slot Thermal Condition Effects on Back-Iron Extension Thermal Benefits," in IEEE Transactions on Transportation Electrification, vol. 7, no. 4, pp. 2927-2938, Dec. 2021, doi: 10.1109/TTE.2021.3085822

[9] A. Boglietti, A. Cavagnino, D. Staton, M. Shanel, M. Mueller and C. Mejuto, "Evolution and Modern Approaches for Thermal Analysis of Electrical Machines," in IEEE Transactions on Industrial Electronics, vol. 56, no. 3, pp. 871-882, March 2009, doi: 10.1109/TIE.2008.2011622.

[10] O. Wallscheid et al., "Global Identification of a Low-Order Lumped-Parameter Thermal Network for Permanent Magnet Synchronous Motors," in IEEE Transactions on Energy Conversion, vol. 31, no. 1, pp. 354-365, March 2016.

[11] H. Zhang et al., "Thermal Model Approach to Multisector Three-Phase Electrical Machines," in IEEE Transactions on Industrial Electronics, vol. 68, no. 4, pp. 2919-2930, April 2021.

[12] Y. Guo, J. Soulard and D. Greenwood, "THERMAL DC TEST AND ANALYSIS OF A STATOR MADE WITH RESIN TRICKLE IMPREGNATION," The 10th International Conference on Power Electronics, Machines and Drives (PEMD 2020), 2020, pp. 467-472, doi: 10.1049/icp.2021.1002.

[13] S. Ayat, H. Liu, M. Kulan and R. Wrobel, "Estimation of Equivalent Thermal Conductivity for Electrical Windings with High Conductor Fill Factor," 2018 IEEE Energy Conversion Congress and Exposition (ECCE), 2018, pp. 6529-6536, doi: 10.1109/ECCE.2018.8557534.

[14] R. Wrobel, G. Vainel, C. Copeland, T. Duda, D. Staton and P. H. Mellor, "Investigation of Mechanical Loss Components and Heat Transfer in an Axial-Flux PM Machine," in IEEE Transactions on Industry Applications, vol. 51, no. 4, pp. 3000-3011, July-Aug. 2015, doi: 10.1109/TIA.2015.2405499.